THE IMPACT OF RESERVOIR CONFINING STRESS ON NMR T2 AND PORE FREQUENCY DISTRIBUTION IN SOME CARBONATE SAMPLES

P Mitchell and M Niedzielak[1], I A Al-Hosani and M Z Kalam[2]
[1]Integrated Core Consultancy Services (UK)
[2]Abu Dhabi Company for Onshore Oil Operations (UAE)

This paper was prepared for presentation at the International Symposium of the Society of Core Analysts held in Calgary, Canada, 10-12 September, 2007

ABSTRACT

Recent developments allow high-pressure mercury intrusion experiments to be performed under reservoir-representative confining stress. NMR relaxation measurements on core samples are increasingly being used in addition to mercury intrusion data since the two techniques yield complementary information about the pore network. Integration of the different measurement techniques result in a more detailed pore network topology at representative conditions.

New apparatus is described in this paper which enables NMR T2 distributions to be determined for core samples under reservoir confining stress. Data for a number of samples originating from two producing carbonate reservoirs are presented. Both high pressure mercury intrusion and NMR relaxation tests were performed at series of increasing confining stresses to observe the transformation in both pore frequency distribution and NMR T2 distribution. Additional core characterisation measurements were performed on the same samples using multi-speed centrifuge at similar confining stresses. The selected reservoir core samples were earlier characterised according to reservoir rock types (RRT) based on conventional poroperm data, ambient condition mercury intrusion data, thin section analysis and X-ray CT scanning.

The systematic changes observed in the pore size and pore throat distributions as a function of increasing confinement is discussed in the context of the different pore space phenomena to which the two types of measurement relate. Comparison between the two methods gives insight into issues such as pore connectivity and accessibility, and the impact on these and other properties as a function of increasing applied stress is also discussed. The results show the importance of representative reservoir core measurements in reducing uncertainty in developed static models and consequent simulation validation for field development models.

INTRODUCTION

High pressure mercury intrusion testing possesses the advantage over gas or oil–brine drainage capillary pressure experiments of great speed of data acquisition at the cost of

not being fully representative due to the non-recognition of wetting film retention (Chetouani et al (2001)). NMR relaxation experiments suffer the same disadvantage but can also be performed quickly, with the added advantages of both testing a larger rock volume than mercury intrusion and being non-destructive. NMR T2 distributions are nowadays often used for rock type characterisation for these reasons.

These two techniques are generally regarded as complementary in nature since both are strongly influenced by the true pore distribution within test specimens without providing a truly definitive measurement. The primary objective of the work reported here is to exploit the complementary nature of these two tests in observing changes in the pore frequency distribution caused by the application of reservoir confining stress. Recently published data show significant systematic transformation in mercury-derived pore frequency distribution as a function of confining stress Mitchell et al (2003). In this paper, the effect of reservoir confining stress on both mercury and NMR-derived distributions is examined for four carbonate core samples originating from Middle-East hydrocarbon producing formations.

EXPERIMENTAL PROCEDURES

A total of four carbonate samples were selected for study, representing two different reservoirs. Off cuts from the samples were subjected to high-pressure mercury intrusion under both ambient conditions and a fixed hydrostatic confining stress of 3200 psi. The confining system used is as described in Mitchell et al (2003) and allows for three-dimensional access of mercury to the test specimen. The experimental protocols and subsequent data manipulation conform to established methods, as described by Shafer et al (2000).

NMR T_2 (transverse relaxation) decay measurements were made using an Oxford Instruments Maran Ultra spectrometer with 75mm probe operating at 35 ^{o}C and 2.2 MHz frequency. The CPMG sequence was used with an inter-echo spacing 0.4ms, 1024 echos and 32 scans. The samples used were 3cm diameter by approximately 2.5cm in length. Prior to making NMR measurements, each plug was cleaned and fully saturated with brine. Each sample was first measured at ambient, and then at a fixed confining stress of 3200 psi using a specially designed hydrostatic vessel made of PEEK (polyetheretherketone) and some other engineering plastics, which were non-sensitive to NMR.

The oil-brine primary drainage tests were conducted under a confining stress of 3200 psi using a Beckman L855M UltraCentrifuge equipped with a PIR 16.5 rotor. A maximum speed of 8000 rpm was used with dead crude as the desaturation medium. The radius to the base of each sample was 8.9 cm.

RESULTS AND DISCUSSION

Analysis of Data

NMR

T_2 distributions were acquired with the WinDXP toolbox, which allows performing distributed exponential fitting of data. The fit is based on the BRD (Butler, Reeds and Dawson) algorithm, as described by Butler et al. (1981). A smoothing parameter (the weight) was calculated using noise estimation. The standard error was used to produce a noise value (based on the signal to noise ratio of the NMR measurement).
The transverse relaxation (T_2) for a single pore can be described by:

$$T_2^{-1} = \rho\,(S/V) \qquad (1)$$

where T_2 is the transverse relaxation, V and S are volume and surface of the pore and ρ is the surface relaxivity parameter.

Numerous authors have attempted to match NMR relaxation time distributions with mercury intrusion pore size distribution including Marshal et al. (1995) and Lowden et al. (1998), since the two methods produce similar cumulative distributions. Our approach for this paper was slightly different in that the direct comparison of interest was drainage capillary pressure curves. We therefore derived relaxivity from a best-fit match between NMR-derived drainage capillary pressure and the centrifuge data over the saturation range covered by the centrifuge, allowing relaxivity to converge to a value corresponding to the least-squares minimisation of saturation difference. A weighting of $1/S_w$ was used to avoid excessive bias in the fit at low capillary pressure when S_w is changing most rapidly. Finally, the conversion from T_2 values to pore diameter was obtained by substituting S/V for cylindrical tube, i.e., S/V = 4/D, into Equation 1. Interfacial tension values of 48 dynes/cm for oil/brine and 485 for mercury / vacuum systems, and contact angles of 30° and 140° respectively.

Mercury Intrusion

Given a fluid [mercury] of surface tension γ and a material containing pore throat of diameter D, the capillary pressure P_c that is required for the fluid to invade the material is given by:

$$P_c = \kappa_1 \frac{\gamma \cos\varphi}{D} \qquad (2)$$

where φ is the contact angle between the fluid and material and κ_1 a unit-dependent constant. The logarithmic pore frequency *F* is defined by:

$$F\left(D_{i+½}\right) = \frac{v_{i+1} - v_i}{\log_{10}\left(D_{i+1}\right) - \log_{10}\left(D_i\right)} \tag{3}$$

where *v* is the cumulative intrusion and *D* is pore throat diameter.

If the diameter of the pore throats is plotted on the x-axis using a logarithmic scale and one decade of the axis is taken as unity, then a scaling factor X for the y-axis can be defined such that one unit of area under the curve ***F(D)*** corresponds to one absolute percentage point of porosity (or "porosity unit").

The factor X is given by:

$$X = \frac{\phi\rho_B}{v_\infty} = \frac{\phi\rho_{g\gamma}}{(1+\phi)v_\infty} \tag{4}$$

where v_∞ is the total volume of mercury injected, ϕ is the sample fractional porosity, ρ_B the bulk density and ρ_{gr} the grain density of the sample.

Centrifuge

The data were processed according to the standard created by Hassler-Brunner (1945). method although taking gradients point-to-point along the Z v $Z.S_w$ curve (where Z is inlet face capillary pressure) was fitted with a functional form whose derived form yields an exponential decay for the capillary pressure curve:

$$Z.S_w = aZ + b - b.\exp(-c.Z) \tag{5}$$

Where a, b and c are fit parameters. The derived form of this equation, which yields the capillary pressure curve is:

$$S_w = a - b.\exp(-c.Z).-c \tag{6}$$

However, allowing for the boundary condition that at Pc (or Z) =0, Sw =1 this enables the parameter c to be defined in terms of the other two leading to the revised version of Eqn. 5:

$$Z.S_w = aZ + b - b.\exp(-Z(1-a)/b) \tag{7}$$

The final equation for the capillary pressure curve is the derivative with respect to Z of Eqn 7 and is:

$$S_w = a - b.\exp(-Z(1-a)/b).-(1-a)/b \quad (8)$$

Note that this substitution has removed one parameter which reduces the equation to a two-parameter fit. This offers a considerable advantage by yielding more degrees of freedom in the fit. This functional form was found to honour the Z v $Z.S_w$ curve exceedingly well.

Thin Sections

The thin sections were prepared on sample offcuts in each case with blue-dyed epoxy and with combined carbonate staining.

Sample Properties

Basic sample properties are presented in Table 1:

Table 1: Summary Sample Properties

Sample	Grain Density	Porosity	Klinkenberg Permeability	Surface Relaxivity
	g/cc	frac	mD	μm/ms
1	2.713	0.124	0.27	0.01907
2	2.712	0.123	0.21	0.01200
3	2.703	0.194	10.0	0.00379
4	2.714	0.170	38.4	0.00922

The selected samples cover a significant range in reservoir quality, with a range in excess of two orders of magnitude in permeability. Recent study shows that the determination of surface relaxivity is often unpredictable, and for carbonates varies by a large factor (Godefroy et al. 1999). The range in derived relaxivity for the subject samples is in the region of a factor of five, although there does appear to be a strong correlation with absolute porosity. However explanations for this such as pore morphology alteration through diagenesis would be speculative for a dataset of this size and in any event is not the subject of this paper.

Sample-Specific Results

A single page has been devoted to the results for each sample comprising a geological description, frequency distribution plots and capillary pressure plots, showing changes as a function of the increasing hydrostatic confining stress regime. An interpretation of the results is also given sample by sample.

Sample 1

Coarse grained intraclastic, skeletal and peloidal packstone and finer grained peloidal packstone, fractured (stylo-fractures), open fractures lined with residual oil and containing coarse crystals of saddle dolomite cement.

Both mercury intrusion and NMR (Figures 1, 2) show some what varimodal distributions although pores in the region of 1 μm are dominant. The impact of stress on the distributions is similar, with a general narrowing and a modest increase in peak height evident. The capillary pressure curves (data determined at reservoir stress shown only) are in good agreement across all three systems over a wide saturation range. Nonetheless in this, as with the other samples, the NMR–derived curve should be viewed as semi-quantitative only since the derivation is dependent uponthe measured oil-brine capillary pressure curve.

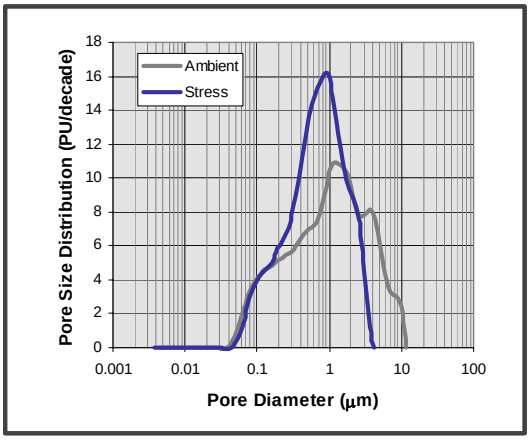

Figure 1 - Pore Throat Size Distribution

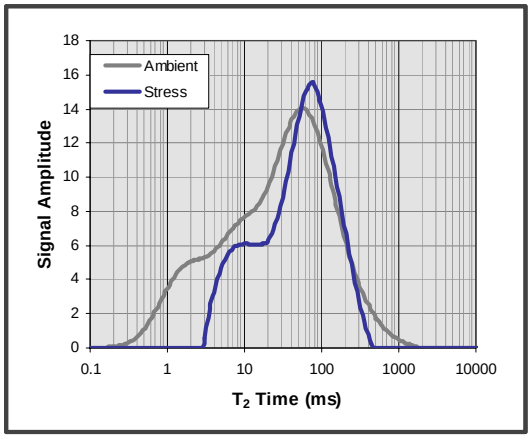

Figure 2 – NMR T2 Distribution

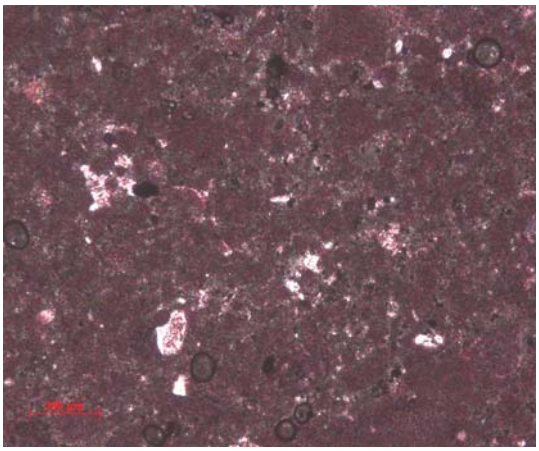

Figure 3 – Thin Section Photograph

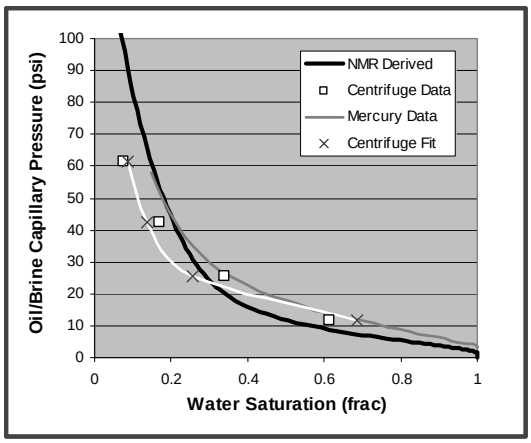

Figure 4 - Capillary Pressure Curves

Sample 2
Skeletal and peloidal packstone, tight, with pellet relics in micrite matrix. Contains Miliolids, and other benthic forams, dasyclads, molluscan and echinoderm fragments.

The shoulders evident on the derived frequency distributions probably reflect the mixture of bioclastic debris present. As with sample 1, the impact of stress causes a sharpening of the distributions (Figure 5, 6) with an associated increase in peak height. In this sample an increased differentiation between micro and intergranular porosity is perceptible at stress. The oil-brine capillary pressure curve (Figure 8) is rather steeper at high drainage pressures than the other two curves, possibly due to some water becoming discontinuous in the centrifuge tests, since there is a tendency towards oil wetness in these carbonate samples.

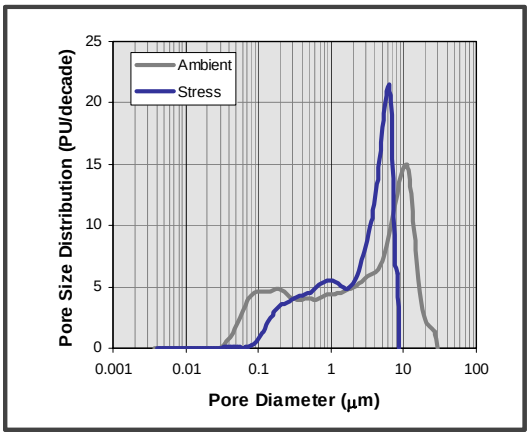

Figure 5 – Pore Throat Size Distribution

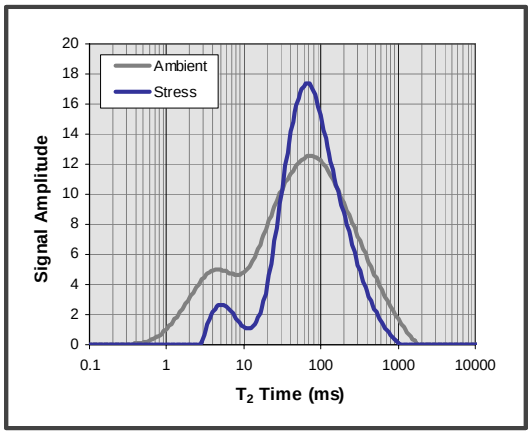

Figure 6 – NMR T2 Distribution

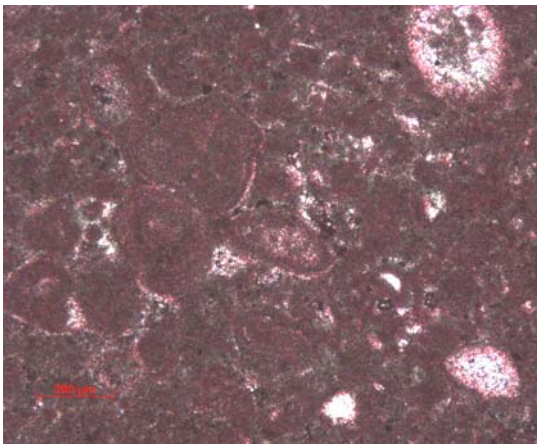

Figure 7 – Thin Section Photograph

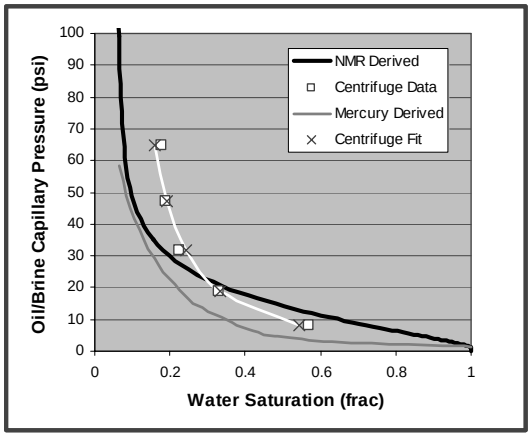

Figure 8 - Capillary Pressure Curves

Sample 3

Fine grained skeletal peloidal packstone to wackestone containing molluscan, echinoderm and dasycladacean debris.

This sample is seemingly almost impervious to the application of confining stress as shown in the minimal alteration in both NMR and mercury distributions due to stress (Figures 9, 10). Both methods also predict strong unimodality. Drainage curves from mercury and NMR are again mutually more compatible than with the centrifuge data (Figure 12) with trapping of water in the centrifuge tests again a possible mechanism for this phenomenon.

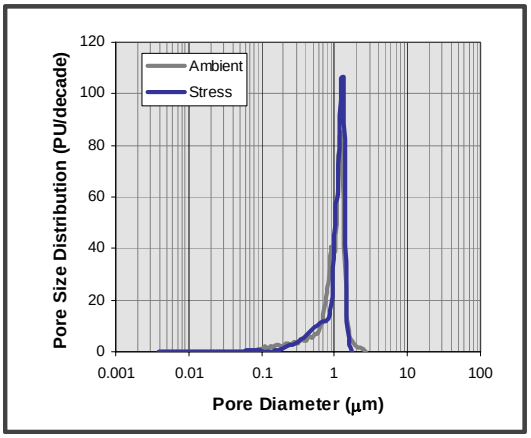

Figure 9 – Pore Throat Size Distribution

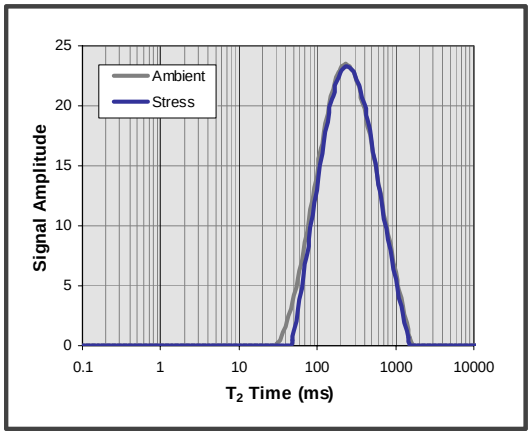

Figure 10 – NMR T2 Distribution

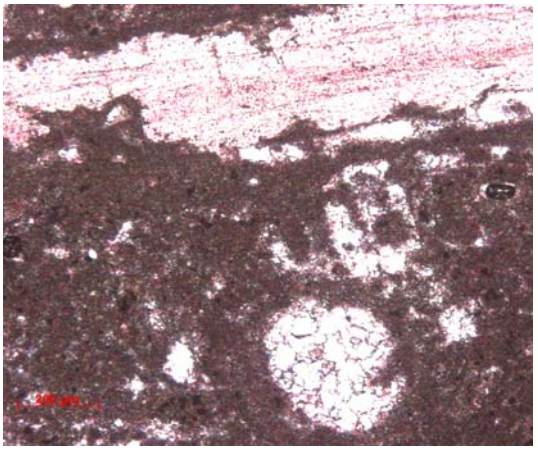

Figure 11 – Thin Section Photograph

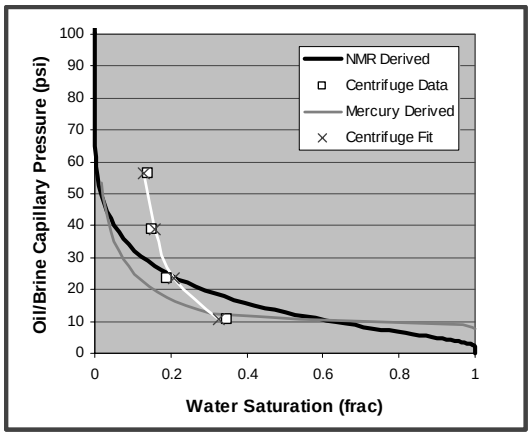

Figure 12 - Capillary Pressure Curves

Sample 4

Intraclastic skeletal and peloidal grainstone with large Orbitolinid benthic forams, smaller Miliolid forams, molluscan and echinoderm debris and dasycladacean grains, now as spar-filled mouldic pores. Some oversized (channel-shaped pores) are lined with meteoric phreatic calcite spar.

The strongly bimodal nature of this sample is evident not only in the frequency distribution plots (Figures 13, 14) but also qualitatively in the thin section photograph (Figure 15). This is clearly a consequence of the division in porosity between inter-granular and intra-granular pores, with both systems showing a separation in pore sizes of more than an order of magnitude. The transformation in derived frequency distributions with stress shares a tendency towards a narrowing of the distributions as seen with the other samples, although this sample differs in that a shift in the modal inter-granular pore size (by NMR) is evident. In this case the NMR-derived capillary pressure curve (Figure 16) is a little different in broad morphology to the other curves, possibly due to the limitations of the NMR curve-fit algorithms in what is clearly a complex pore frequency distribution.

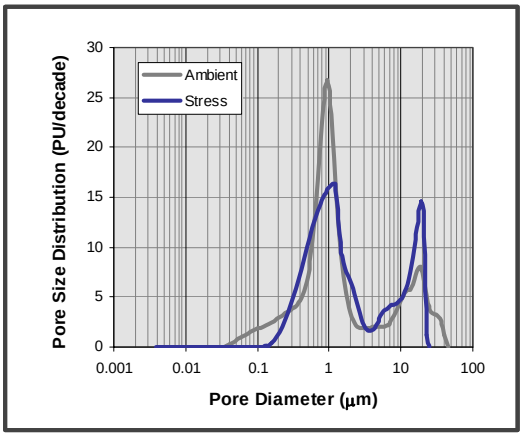

Figure 13 - Pore Throat Size Distribution

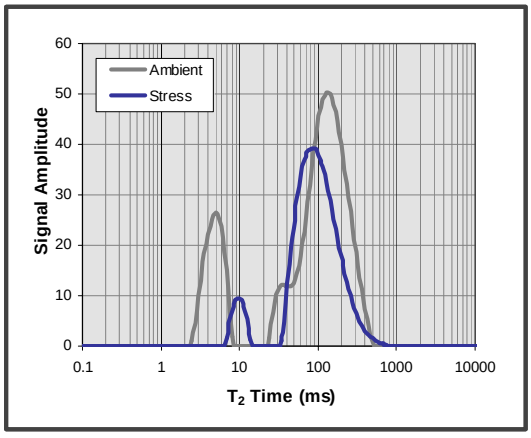

Figure 14 – NMR T2 Distribution

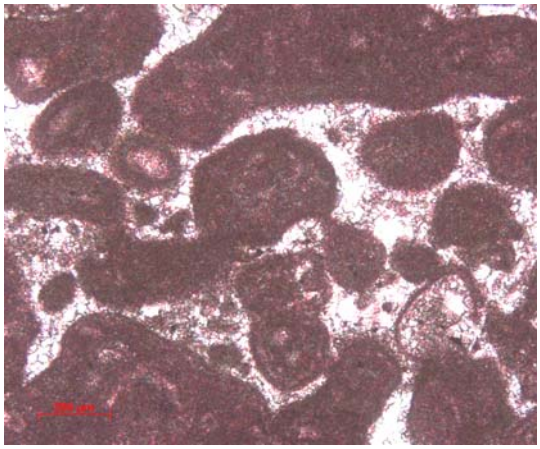

Figure 15 – Thin Section Photograph

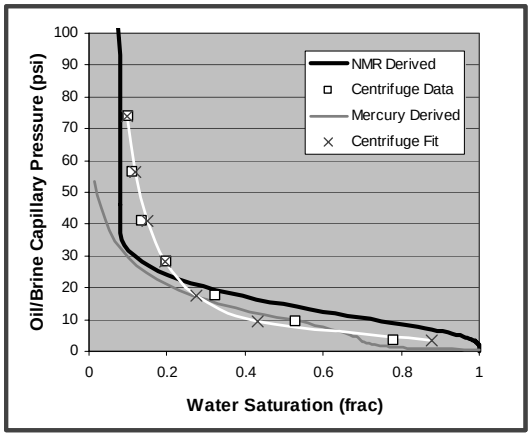

Figure 16 - Capillary Pressure Curves

CONCLUSIONS

1. The transformations seen in the frequency distributions derived from NMR and mercury intrusion due to the application of stress are generally comparable in qualitative terms, although modal pore size as predicted by NMR tests appears to be less altered by the application of stress than with mercury data.

2. Some loss of microporosity at stress is a feature of both the mercury intrusion and NMR tests suggesting that this phenomenon is real and not the result of pore occlusion, however further work is required to reach a definitive conclusion.

3. The capillary pressure curves derived from mercury intrusion and NMR appear to be mutually somewhat more compatible than with the centrifuge data suggesting some fundamental commonality between these two systems.

4. The variation in derived surface relaxivity as derived by comparing mercury intrusion and NMR data is large for the samples tested and mirrors observations elsewhere in the literature. This has implications in terms of seeking to derive properties such as permeability and drainage capillary pressure from NMR data.

ACKNOWLEDGEMENTS

The authors wish to acknowledge the Abu Dhabi Company for Onshore Operations (ADCO) and Abu Dhabi National Oil Company (ADNOC) for granting permission to publish the data contained in this paper.

REFERENCES

Chetouani, N. and Mitchell, P.: "The effect of pore structure on primary drainage capillary behaviour", *International Symposium of the Society of Core Analysts*, (**2001**) SCA 2001-47.

Mitchell, P., Sincock K. and Williams, J.: "On the effect of reservoir confining stress on mercury intrusion-derived pore frequency distribution", *International Symposium of the Society of Core Analysts*, (**2003**) SCA 2003-23.

Shafer, J., and Neasham, J.: "Mercury Porosimetry Protocol for Rapid Determination of Petrophysical and Reservoir Quality Properties", *International Symposium of the Society of Core Analysts*, (**2000**) SCA 2021.

Marschall, D., Gardner J. S., Mardon, D., Coates, G. R.: "Method for correlating NMR relaxometry and mercury injection data", *International Symposium of the Society of Core Analysts*, (**1995**) SCA 9511.

Lowden, B.D., Porter, M. J., Powrie, L. S.: "T_2 relaxation time versus mercury injection capillary pressure: Implications for NMR logging and reservoir characterisation", *Society of Petroleum Engineers*, **(1998)** SPE 50607.

Butler, J.P., Reeds, J. A., Dawson, S. V.: *SIAM J. Numer. Anal*. **18**. 381 (1981).

Godefroy, S., Korb, J.-P., Petit, D., Fleury, M.: “NMR surface relaxivity and diffusion effects in grain packs” *International Symposium of the Society of Core Analysts*, (**1999**) SCA 9920.
Hassler, G.L., Brunner,E., “Measurement of Capillary Pressure in Small Core Samples”, *Trans. AIME*, **1945,** 160, 114-123